Reactions $pd \rightarrow {}^3\mathrm{He}\,\eta$ and $pd \rightarrow {}^3\mathrm{He}\,\pi^+\pi^-$ near the η threshold

B. Mayer, A. Boudard, B. Fabbro, M. Garçon, C. Kerboul, J. Poitou, and F. Wellers
Service de Physique Nucléaire, CEA Saclay, F-91191 Gif-sur-Yvette, France

W. W. Jacobs,* J. Saudinos, and E. Tomasi-Gustafsson
Laboratoire National Saturne, F-91191 Gif-sur-Yvette, France

J. P. Mouly
Service d'Etudes des Détecteurs, CEA Saclay, F-91191 Gif-sur-Yvette, France

R. S. Kessler, B. M. K. Nefkens, and B. Tippens
Department of Physics, University of California, Los Angeles, California 90024

A. van der Schaaf
Physik-Institut der Universität Zürich, CH-8057 Zürich, Switzerland

R. Abegg and W. T. H. van Oers
TRIUMF, 4004 Wesbrook Mall, Vancouver, British Columbia, Canada V6T 2A3

W. Briscoe and A. Petrov
Center for Nuclear Studies and Department of Physics, The George Washington University, Washington, D.C. 20052

A. Moalem
Department of Physics, Ben Gurion University, Beer-Sheva 84105, Israel
(Received 26 October 1995)

The reaction $pd \rightarrow {}^3\mathrm{He}\,\eta$ has been studied with the SPES2 spectrometer, for proton energies between 0.2 MeV and 11 MeV above threshold. The total cross section rises from 0.25 to 0.40 μb in this region. The observed energy dependence can be attributed to the strong final state interaction. The angular distribution is nearly isotropic, consistent with S wave production. A measurement of the $pd \rightarrow {}^3\mathrm{He}\,\pi^+\pi^-$ cross section in the threshold region is also presented. The setup, which is capable of producing 10^5 tagged η/s with only a few percent background, is used to investigate rare η decays. [S0556-2813(96)01405-7]

PACS number(s): 25.40.Ve, 13.75.Cs, 14.40.Aq, 21.45.+v

I. INTRODUCTION

Earlier measurements at the Laboratoire National Saturne, at Saclay, have revealed a surprisingly large cross section for the $pd \rightarrow {}^3\mathrm{He}\,\eta$ reaction, around 0° in the laboratory, near threshold [1]. A three-body mechanism has been proposed [2, 3] in which the rescattering of an intermediate pion allows the sharing of the high momentum transferred. The N^* (1535) resonance, which strongly couples to the $N\eta$ system, should also play an important role.

The $pd \rightarrow {}^3\mathrm{He}\,\eta$ reaction is of interest as a source of η, tagged by the recoil ^{3}He. Near threshold the ^{3}He particles are emitted in a narrow forward cone and the tagging can be done with high efficiency in a magnetic spectrometer. Such a source of tagged η is indeed of considerable interest, since the η decay modes could be studied with a precision similar to those of the other light pseudoscalar mesons π and K. In most previous experiments the η mesons were produced through the $\pi^- p \rightarrow \eta n$ reaction with low intensity and high physical background.

As the central part of the new tagged η facility, the SPES2 spectrometer was installed at the Saturne II synchrotron. The $pd \rightarrow {}^3\mathrm{He}\,\eta$ cross section was measured at eight different proton energies from 0.2 to 11 MeV above threshold. Only the ^{3}He particles were detected, with the spectrometer positioned at 0° (see Fig. 1). Preliminary results have been presented at various conferences [4]. The results of the complete analysis, including the angular distributions, are discussed here.

In a next step a double-arm pion detection system has been added and the reaction $pd \rightarrow {}^3\mathrm{He}\,\pi^+\pi^-$ was studied. The aim was to investigate the ρ contribution and a possible threshold effect at the opening of the η channel.

II. THE EXPERIMENTAL METHOD

The proton beam, with a momentum dispersion of 4×10^{-4} (FWHM) and an intensity around 10^{10} particles per burst of 400 ms, every 1.2 s, was focused on the liquid deuterium target to a spot of 2×2 mm^2. The beam divergence was 3 mrad both vertically and horizontally. The beam intensity was monitored 1 m upstream of the LD_2 target with two plastic scintillation telescopes viewing a thin polypro-

*On leave from Indiana University Cyclotron Facility and Department of Physics, Bloomington, Indiana 47408.

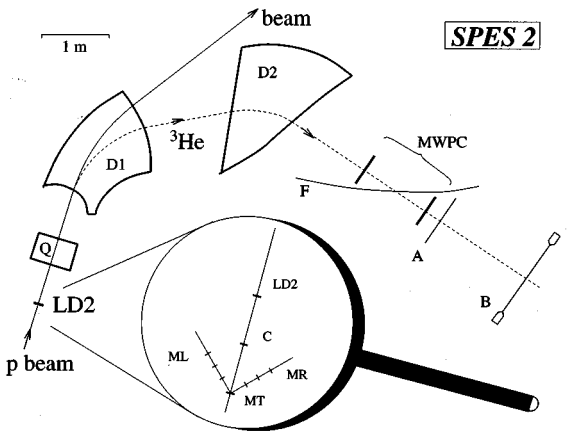

FIG. 1. Top view of the experimental setup. LD_2 is the liquid deuterium target, MT is a thin polypropylene monitor target, *ML* and *MR* are two telescopes of scintillators, *C* is a retractable ^{12}C target used for absolute normalization, *Q* is a quadrupole magnet, *D*1 and *D*2 are dipole magnets, *F* represents the focal surface of the spectrometer, MWPC are two multiwire proportional chambers, hodoscope *A* and counter *B* are plastic scintillators.

pylene target at $\pm 40°$. Two monitor targets (8 μm and 20 μm thick) were selected depending on the beam intensity. The monitors were calibrated with an accuracy of $\pm 5\%$ by irradiating a ^{12}C target for a known period of time, and measuring the ^{11}C activity formed via the (p,pn) reaction [5].

The liquid deuterium target assembly consisted of two identical rectangular cells (70 mm $\times$ 25 mm), 7 mm thick, one filled and the other one empty. The cells were mounted one above the other and could be moved up and down. They were wrapped in 10 layers of 3 μm thick aluminized mylar for thermal insulation. The windows were made of 50 μm thick Mylar and the energy loss in the target was 0.37 MeV/cm for the incident protons and 5.0 MeV/cm for the outgoing ^{3}He.

The recoiling ^{3}He, emitted in forward direction, were analyzed in the SPES2 spectrometer [6], which consists of a vertically focusing quadrupole and two dipoles. The distance between the target and the quadrupole was 60 cm (114 cm in the case of the $pd \to {}^3\mathrm{He}\pi^+\pi^-$ reaction study). The spectrometer vacuum was separated from the vacuum region around the target by a 10 μm thick Mylar foil and maintained up to the exit window of the second dipole. When the spectrometer was adjusted to direct the ^{3}He particles to the focal plane, the proton beam passed between the two dipoles and left the spectrometer through a special window until it reached the beam dump.

The detection system consisted of two multiwire proportional chambers with two wire planes each, followed by two layers of plastic scintillation counters, ''*A*'' and ''*B*'' in Fig. 1. The wire chambers are square, each plane having 256 wires with 2 mm spacing. Since the spatial distribution of the particles reaching the chambers is much wider horizontally than vertically, the wires were oriented at $\pm 45°$ in order to distribute the flux over a larger number of wires. The wire chambers were filled with a gas mixture of 75% argon and 25% isobutane (no freon was used) and read out with PCOS III electronics. Thanks to the large energy loss of the ^{3}He particles, the chambers could be operated at low gain to make them insensitive to protons and pions.

The *A* array of 8 plastic scintillators (8 $\times$ 10 $\times$ 0.4 cm^3 each) was separated from the single *B* scintillator (120 $\times$ 20 $\times$ 1 cm^3) by 150 cm, corresponding to a flight time of $\approx$10.7 ns for ^{3}He particles and $\approx$13.6 ns for deuterons. Scintillator *B* was viewed by a photomultiplier at each end to reduce the position dependence of the light collection. The discriminator thresholds were set above the signal amplitudes of pions, protons, and most deuterons reaching the scintillators. The time delay between crossings in *A* and *B* was measured with a resolution of typically 1.0 ns (FWHM).

SPES2 was set to accept forward angles up to 3° horizontally and 6° vertically and momenta/charge of 650 MeV/c $\pm 10\%$. The trigger for data readout was a simple coincidence between *A* and *B* counters. Still at 2 MeV above threshold, for example, the trigger rate was only twice the rate of reconstructed $pd \to {}^3\mathrm{He}\,\eta$ events.

III. ANALYSIS AND RESULTS

The proton energy above threshold, ΔT_p, is given by

$$\Delta T_p \equiv T_p - T_p^{\mathrm{thresh}}, \tag{1}$$

with T_p the proton kinetic energy and $T_p^{\mathrm{thresh}} = 891.37$ MeV its value at threshold. For the small values of ΔT_p, studied in the present work, the following approximations may be used (ΔT_p in MeV, θ in degrees):

$$\frac{p_{\mathrm{He}}^{\mathrm{max}} - p_{\mathrm{He}}^{\mathrm{min}}}{\overline{p_{\mathrm{He}}}} = 0.038\sqrt{\Delta T_p}, \tag{2}$$

$$\theta_{\mathrm{He}}^{\mathrm{max}} = 0.99\sqrt{\Delta T_p}, \tag{3}$$

$$\theta_{\eta}^{\mathrm{max}} = 5.05\sqrt{\Delta T_p}, \tag{4}$$

where $\overline{p_{\mathrm{He}}}$, $p_{\mathrm{He}}^{\mathrm{min}}$, and $p_{\mathrm{He}}^{\mathrm{max}}$ are the mean, minimum, and maximum values of the ^{3}He momentum, respectively, whereas $\theta_{\mathrm{He}}^{\mathrm{max}}$ and $\theta_{\eta}^{\mathrm{max}}$ are the maximum values for the ^{3}He and η laboratory angles. A systematic expansion of kinematical variables near threshold can be found in [7].

At each beam energy the analysis involved the following steps: ^{3}He selection and momentum determination, extraction of ΔT_p from the ^{3}He momentum distribution, and determination of the total cross section and the forward-backward asymmetry.

A. ^{3}He selection and momentum determination

The ^{3}He particles were selected by cuts on energy loss and time of flight as shown in Fig. 2. The cuts are large enough not to lose ^{3}He particles. Small contaminations by other particles are properly taken into account in the background subtraction discussed below. Since the geometric acceptance of the chambers is larger than that of the ''*A*'' hodoscope, the reconstruction efficiency is given by the number of reconstructed tracks divided by the number of events that satisfy the ^{3}He selection. The efficiency for the reconstruction of the ^{3}He trajectories was 74–78 %. The inefficiency was mostly due to nonadjacent, but nearby, hit wires that resulted in ambiguous tracks.

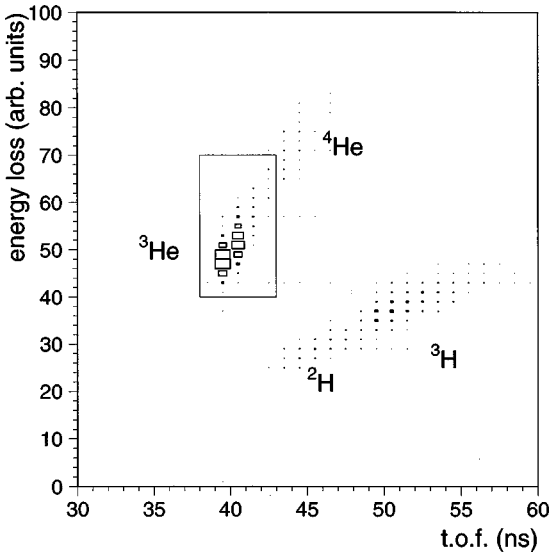

FIG. 2. Distribution of the energy loss in A counters vs time of flight from A to B. The box shown was used to select the ^{3}He particles.

The ^{3}He emission angles θ_h and θ_v at the target and the normalized momentum $\delta_{\rm He}$, defined as

$$\delta_{\rm He} \equiv \frac{p_{\rm He} - \overline{p_{\rm He}}}{\overline{p_{\rm He}}}, \tag{5}$$

were calculated from the measured trajectories, using the SPES2 transfer matrix elements 0.315%/cm for the inverse momentum dispersion, -2.35 and -0.181 for the inverse horizontal and vertical magnifications, respectively, and $d\theta_v/dy_{\rm FOC} = 13.0$ mrad/cm, where $y_{\rm FOC}$ is the vertical coordinate at the focal plane. The resolution for θ_v (1.5° FWHM) is poorer than the one for θ_h (0.5° FWHM) as a consequence of the smaller magnification. The momentum resolution of 0.5% FWHM is dominated by the spread in energy loss in the target.

Typical spectra of $\delta_{\rm He}$, θ_h and θ_v are shown in Fig. 3. As mentioned above, the widths of these distributions varies in proportion to $\sqrt{\Delta T_p}$. At $\Delta T_p = 2$ MeV and for the software cuts indicated in Fig. 3(d), the background amounts to 10%. Half of it originates in beam interactions in the target windows, as studied with the empty target cell. At larger values of ΔT_p the larger phase space results in increased background.

The background distribution for $\delta_{\rm He}$ was measured at 1 MeV below threshold, and subtracted from the full $\delta_{\rm He}$ spectra after normalization in the region outside the $pd \rightarrow {}^3{\rm He}\eta$ peak (Fig. 4). This procedure, in which the background shape is assumed not to change near threshold, is believed to be valid since the below threshold spectrum perfectly matches the above threshold ones outside the central bump. The resulting $\delta_{\rm He}$ distributions were used to determine ΔT_p, the total cross section and forward-backward asymmetry.

B. Determination of ΔT_p

ΔT_p was obtained by fitting the ^{3}He momentum spectra with a Monte Carlo simulation, minimizing

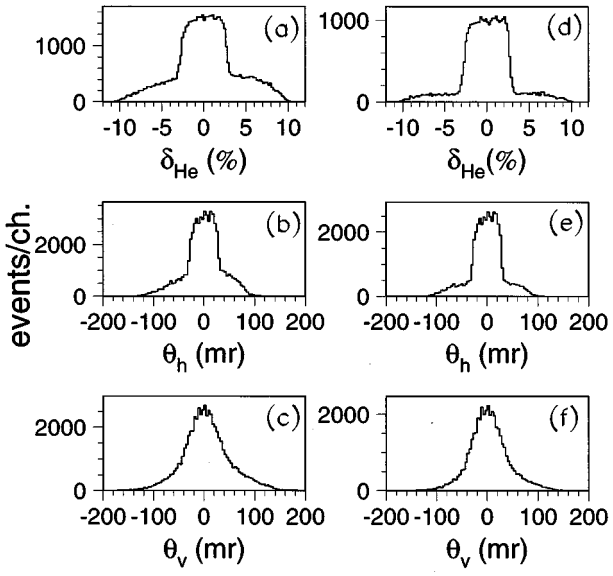

FIG. 3. ^{3}He spectra, at $\Delta T_p = 2$ MeV, for (a) $\delta_{\rm He}$, defined in Eq. (5), (b) θ_h, the horizontal emission angle, (c) θ_v, the vertical emission angle, and spectra with cuts (d) $\delta_{\rm He}$ with $|\theta_h| \leq 40$ mrad and $|\theta_v| \leq 40$ mrad, (e) θ_h with $|\delta_{\rm He}| \leq 3.8$, (f) θ_v with $|\delta_{\rm He}| \leq 3.8$. The background in (d) is 10%.

$$\chi^2 = \sum_i \frac{(N_i^{\rm MC} - N_i^{\rm expt})^2}{\sigma_i^2}, \tag{6}$$

where i is the ith momentum bin, $N_i^{\rm MC}$ and $N_i^{\rm expt}$ are the contents of the ith momentum bin, for the Monte Carlo simulation and for the experiment, respectively. The GEANT based simulation took into account the beam dispersion in momentum, the loss of energy and the straggling in momen-

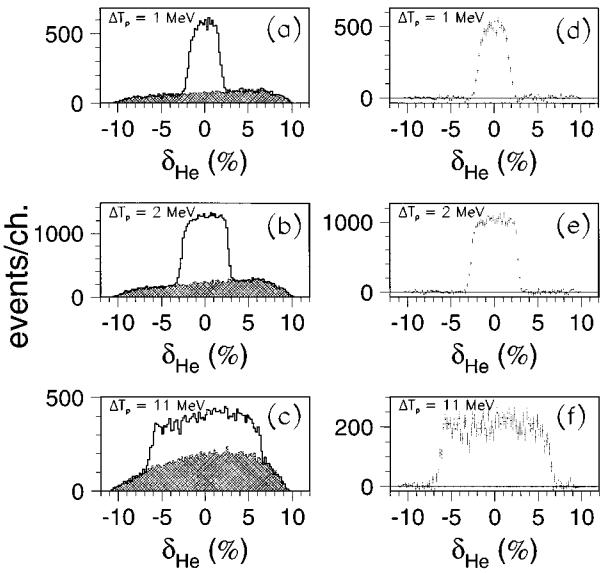

FIG. 4. $\delta_{\rm He}$ spectra at three different beam energies. (a) $\Delta T_p = 1$ MeV, with $|\theta_h| \leq 36$ mrad, (b) $\Delta T_p = 2$ MeV, with $|\theta_h| \leq 40$ mrad and (c) $\Delta T_p = 11$ MeV, with $|\theta_h| \leq 84$ mrad; in grey is the below threshold spectrum normalized to match the region outside the ^{3}He peak for the above threshold spectra. (d)–(f) show the corresponding spectra after background subtraction.

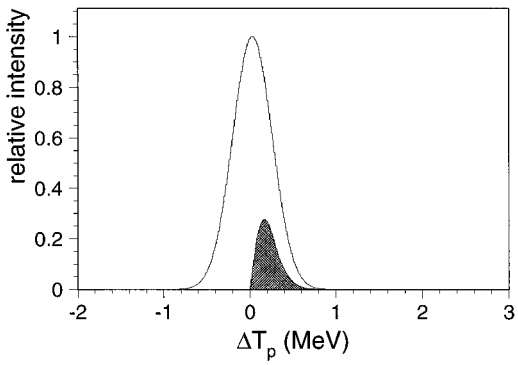

FIG. 5. ΔT_p distributions for incident protons (unshaded) and for protons producing η (in grey), for the lowest energy run.

tum and angle for both incident protons and emitted ^{3}He. The spectrometer response was described by a first-order transfer matrix.

The 1% uncertainty in the momentum dispersion of SPES2 gave a systematic error in ΔT_p of $0.02\times\Delta T_p$, which was added in quadrature to the statistical error.

For the lowest energy point, the cross section cannot be assumed to be constant within the small beam energy dispersion, as is implicit in Eq. (6); a cross section proportional to the η momentum in the c.m. was then assumed to determine ΔT_p. Moreover, for the lowest energy point, most of the beam slowed down to below threshold energy and could not undergo the $pd\rightarrow{}^3\mathrm{He}\,\eta$ reaction; ΔT_p was -0.1 MeV in the middle of the target. Therefore corrections for effective energy and target thickness were applied. The effective energy distribution of protons producing η is given by

$$D_\eta(\Delta T_p)=\int_0^l \exp\left\{-\left[T_p-\left(T_p^0-x\frac{dT}{dx}\right)\right]^2\Big/2\sigma_T^2\right\}dx, \tag{7}$$

with

$$l=\min\left(L_{\text{target}},\frac{\Delta T_p}{dT/dx}\right), \tag{8}$$

and T_p^0 the mean value of T_p and $\sigma_T=0.23\pm0.08$ MeV.

Figure 5 shows the resulting $D_\eta(\Delta T_p)$ distribution, which corresponds to an effective value of $\Delta T_p=(0.22\pm0.07)$ MeV. The error is mainly given by the uncertainty in σ_T and not so much by details of the beam shape; for a parabolic shape with the same σ_T value, ΔT_p changes by less than 3%.

C. Total cross section and forward-backward asymmetry

The measured total cross sections are presented in Table I and Fig. 6. The errors include statistical errors and a systematic error of 2% which reflects the uncertainty in background subtraction and beam monitoring. The reconstructed vertical position spectra at planes *A* and *B* showed that there was no loss of acceptance. For the lowest energy run, an effective target thickness was calculated as mentioned above. Also here the main error source is the uncertainty in σ_T, which leads to asymmetric error bars. A global normalization error of $\pm7\%$ arises from $\pm5\%$ uncertainties in both the beam intensity and the target thickness. Losses of ^{3}He particles, due to nuclear reactions along their path, were neglected.

TABLE I. Total cross section for $pd\rightarrow{}^3\mathrm{He}\,\eta$ as a function of ΔT_p. Errors are discussed in the text. They do not include the 7% overall normalization error.

ΔT_p	(MeV)	σ_{tot}	(μb)
0.22	±0.07	0.225	$+0.04$
			-0.02
0.93	±0.03	0.351	±0.012
1.99	±0.04	0.409	±0.011
3.32	±0.07	0.424	±0.012
4.90	±0.11	0.429	±0.015
6.90	±0.15	0.431	±0.015
8.80	±0.20	0.404	±0.018
11.02	±0.26	0.404	±0.018

Figure 4 shows that the δ_{He} spectra are flat at all measured beam energies, which reflects an isotropic angular distribution in the c.m. system. A forward-backward asymmetry $A_{\text{c.m.}}$ is defined as:

$$\frac{d\sigma}{d\Omega_{\text{c.m.}}}=\frac{\sigma_{\text{tot}}}{4\pi}[1+A_{\text{c.m.}}\cos\theta_{\text{c.m.}}]. \tag{9}$$

The asymmetry $A_{\text{c.m.}}$ was determined by minimizing the χ^2 in Eq. (6), with respect to $A_{\text{c.m.}}$. As a consistency check $A_{\text{c.m.}}$ was also determined for restricted regions of δ_{He}. The resulting $A_{\text{c.m.}}$ values, shown in Fig. 7, are consistent with zero to within 5% at all energies.

IV. DISCUSSION OF THE REACTION $pd\rightarrow{}^3\mathrm{He}\,\eta$

The angular dependence of the cross section for the reaction $pd\rightarrow{}^3\mathrm{He}\,\eta$ differs strongly from the one for $pd\rightarrow{}^3\mathrm{He}\,\pi^0$. In the latter, large asymmetries were observed close to threshold, which have been attributed to the *P* wave component interfering with the *S* wave [8]. An isotropic distribution, as observed for the $pd\rightarrow{}^3\mathrm{He}\,\eta$ reaction, is characteristic for pure *S* wave production.

Also the energy dependence of the total cross section near threshold differs strongly in these two reactions. The total

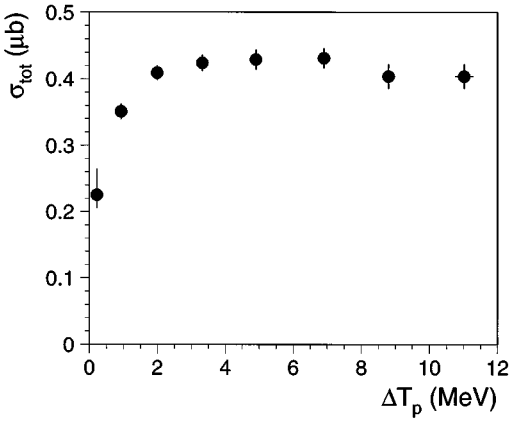

FIG. 6. Total cross section for $pd\rightarrow{}^3\mathrm{He}\,\eta$ as a function of ΔT_p. The error bars do not include the global normalization error.

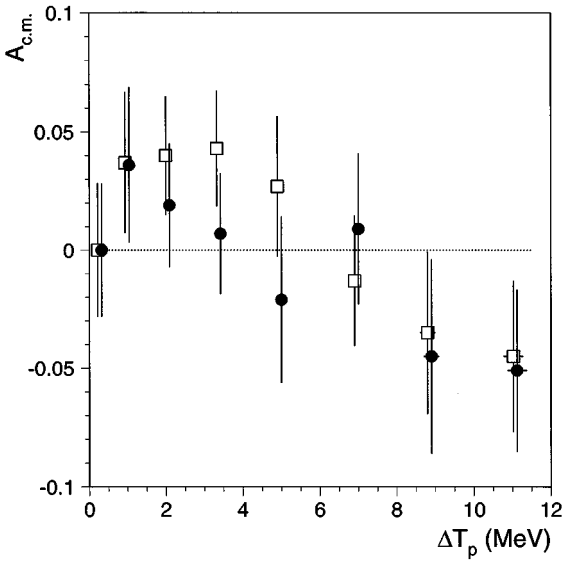

FIG. 7. Forward-backward asymmetry $A_{\text{c.m.}}$ for the $pd\rightarrow{}^3\text{He}\eta$ cross section. The solid square data points were obtained from the full δ_{He} spectra, the solid circle data points from the δ_{He} spectra after removing the edges. A 2% systematic error, introduced for possible variation of detection efficiency along the focal surface, has been added to the statistical error in quadrature.

cross section for the $pd\rightarrow{}^3\text{He}\pi^0$ reaction increases rapidly from threshold to at least 30 MeV above threshold [8], whereas for $pd\rightarrow{}^3\text{He}\eta$, the total cross section rises sharply, within 2 MeV, and then remains almost constant, at least up to 11 MeV. To explain this behavior Wilkin [9] suggested a mechanism in which the energy dependence of the cross section for $pd\rightarrow{}^3\text{He}\eta$ results from the strong final state interaction. The $\eta{}^3$He interaction originates from the strong ηN S wave interaction dominated by the $N^*(1535)$ resonance. For the $pp\rightarrow pp\eta$ reaction also, the cross section, near threshold, seems to be accounted for by the final state interaction involving the $N^*(1535)$ resonance [10].

Taking out kinematic factors, an amplitude f is defined with

$$|f|^2=\frac{p_p}{p_\eta}\frac{d\sigma}{d\Omega_{\text{c.m.}}}, \tag{10}$$

where p_p and p_η are the proton and η momenta in the c.m. system. Whereas $|f|^2$ drops rapidly for increasing p_η in the case of $pd\rightarrow{}^3\text{He}\eta$ (Fig. 8), it remains almost constant for $pd\rightarrow{}^3\text{He}\pi^0$ [8].

In the case of a strong final state interaction, in an S wave, f can be approximated in our limited energy range near threshold by [11]

$$f=\frac{f_B}{1-ip_\eta a}, \tag{11}$$

where f_B is a normalization factor and a is the $\eta{}^3$He scattering length. A fit to our data gives

$$|\text{Re}(a)|=3.8\pm0.6\text{ fm}, \tag{12}$$

$$\text{Im}(a)=1.6\pm1.1\text{ fm}, \tag{13}$$

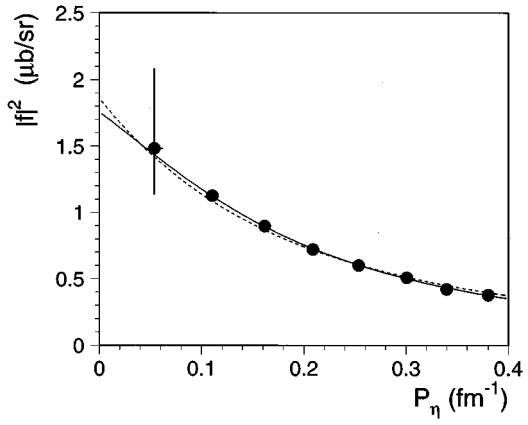

FIG. 8. The square of the $pd\rightarrow{}^3\text{He}\eta$ amplitude defined by Eq. (10), as a function of the η momentum in the c.m. Both curves were calculated with Eq. (11). The solid curve is a fit obtained with the scattering length of Eqs. (12) and (13); the dashed curve is the prediction of Ref. [9] with the scattering length of Eq. (14).

compared to

$$a=(-2.3+i\,2.6)\text{ fm}, \tag{14}$$

obtained through a rough calculation using an $\eta{}^3$He optical potential [9]. The agreement of this simple model with the data is quite remarkable. As mentioned in Ref. [9], the values of Re(a) and Im(a) found by fitting the data are largely correlated, but this does not affect the conclusion regarding a large $\eta{}^3$He scattering length. In recent calculations [12] a two-step model was applied, where a pion emitted in the $NN\rightarrow d\pi$ reaction, produces an η via the $\pi N\rightarrow\eta N$ reaction on the second nucleon. Again the conclusion is that the energy dependence of the cross section is dominated by the final state interaction.

V. THE REACTION $pd\rightarrow{}^3\text{He}\pi^+\pi^-$

The reaction $pd\rightarrow{}^3\text{He}\pi^+\pi^-$ was studied with the setup built for the measurement of the $\eta\rightarrow\mu^+\mu^-$ branching ratio [13]. The aim was to search for a threshold effect at the opening of the η channel, as has been observed in other reactions [14], and to estimate the ρ background below the η signal (see Fig. 3). The ρ mass is 770 MeV/c^2 and its width is 150 MeV/c^2, so there could be a contribution in the region around the η mass. In some decay channels the ρ contribution is strongly enhanced relative to the η contribution. A search for the CP violating $\eta\rightarrow\pi^+\pi^-$ decay, for instance, would suffer considerably from ρ background.

The experimental setup is described in detail in Ref. [13]. The pions were detected with two plastic scintillation detectors, positioned at angles $\pm63°$ corresponding to $\approx90°$ in the center of mass. Each detector consisted of a horizontal and vertical hodoscope which gave the emission angles. The absorbers mentioned in Ref. [13] had been removed. The measurements were done at eight incident energies from $\Delta T_p=-5.26$ to $\Delta T_p=4.65$ MeV. Events were recorded in which a ^{3}He particle in SPES2 was detected in coincidence with signals in both pion detectors. Above the η threshold, the beam energy was deduced from the ^{3}He momentum

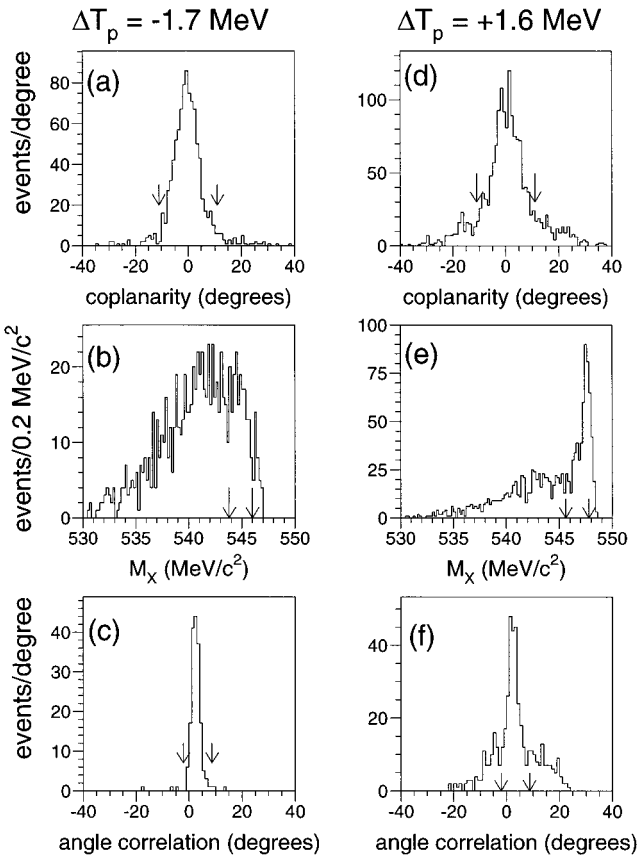

FIG. 9. (a) Coplanarity [angle between the (X,π^+) and the (X,π^-) planes] spectrum, at $\Delta T_p=-1.7$ MeV; the $pd\rightarrow{}^3\mathrm{He}\pi^+\pi^-$ events were selected by cutting events outside the region defined by the two arrows; (b) missing mass spectrum for the $pd\rightarrow{}^3\mathrm{He}X$ reaction, with the coplanarity cut in (a); the arrows show the missing mass band selected; (c) opening angle (measured minus calculated) distribution with both coplanarity and M_X cuts; the arrows define the selected band for cross section calculation. (d)–(f) are the corresponding spectra at $\Delta T_p=1.6$ MeV.

spectrum [Eq. (2)]. At lower energies the beam momentum was scaled to the main magnetic field of the accelerator. For each event the missing mass M_X for the $pd\rightarrow{}^3\mathrm{He}X$ reaction was calculated from the ^{3}He kinematic variables and ΔT_p. Then a 2.2 MeV/c^2 wide band of missing mass, 0.4 MeV/c^2 below the maximum missing mass (Fig. 9) was selected ($M_{\max}-2.6\leqslant M_X\leqslant M_{\max}-0.4$). This choice of missing mass band was such that the reaction $pd\rightarrow{}^3\mathrm{He}X$ occurred close to threshold. This ensured that there was no cut in phase space since the ^{3}He were then emitted in a narrow cone. The 2.2 MeV/c^2 width of the strip was chosen because it is roughly the width of the η missing mass peak at its base. The central value of M_X varies from 542.9 MeV/c^2 to 548.4 MeV/c^2 in the above-mentioned energy range.

The next step in the analysis was the reduction of the background coming from $pd\rightarrow{}^3\mathrm{He}\pi^+\pi^-\pi^0$, $pd\rightarrow{}^3\mathrm{He}\pi^+\pi^-\gamma$, and from the target cell windows. Since one considers a small band of missing mass M_X, one can use the kinematical properties of $pd\rightarrow{}^3\mathrm{He}X$ followed by the ''decay'' of the object X into $\pi^+\pi^-$. As discussed in more detail in Ref. [13], there are two constraints on the $\pi^+\pi^-$ decay angles: coplanarity of the X, π^+ and π^- trajectories,

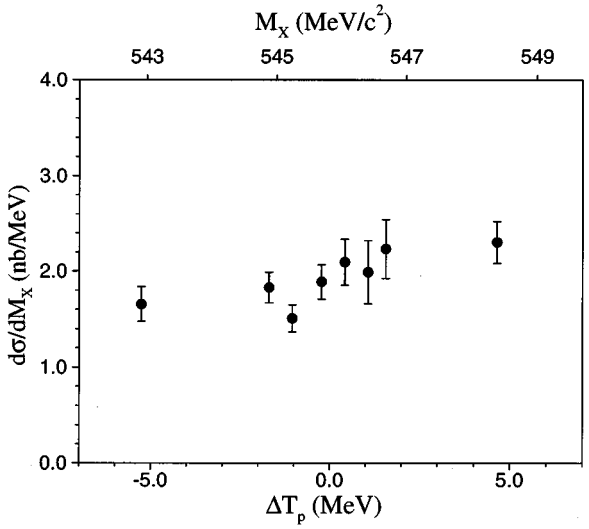

FIG. 10. Cross section for $pd\rightarrow{}^3\mathrm{He}\pi^+\pi^-$ near the $pd\rightarrow{}^3\mathrm{He}\eta$ threshold, as a function of both the incident energy and the missing mass M_X (invariant mass of the two pions).

and the angular correlation between the two pions. After applying these constraints (Fig. 9) and subtracting the background, the cross section for $pd\rightarrow{}^3\mathrm{He}\pi^+\pi^-$ was determined for the chosen values of M_X, taking into account the limited acceptance of the hodoscope detectors (2.9%, almost constant over the whole energy range), and assuming that the pions have an isotropic distribution in their center of mass.

The results shown in Fig. 10 indicate a smooth variation of the cross section with energy and/or missing mass M_X. No threshold effect is seen at the opening of the η channel. For $\Delta T_p=1.5$ MeV, the standard energy for the use of SPES2 as a tagged η facility, the $^3\mathrm{He}\pi^+\pi^-$ production rate (with $\Delta M_X=2.2$ MeV/c^2) would be 1.3% of the η production, if the reaction were isotropic. If the two pions originate from a ρ, then the nonisotropic c.m. angular dependence could result in a two-pion contribution that is larger than 1.3%. The amplitudes for producing a ρ in $m=0$ and $m=\pm1$ spin states are indeed independent at threshold [15]. The ρ decay contribution is therefore not necessarily isotropic in the center of mass of the pion pair but is of the form $a\sin^2\theta+b\cos^2\theta$, where a and b are positive. Since the measurement was done at 90° in the center of mass, the result is sensitive to the a factor only.

VI. CONCLUSION

The present measurement of the $pd\rightarrow{}^3\mathrm{He}\eta$ reaction for proton energies up to 11 MeV above threshold, shows that, in this kinematic region, the angular distributions are consistent with S wave production. The reaction differs strongly from the $pd\rightarrow{}^3\mathrm{He}\pi^0$ reaction where the P wave component contributes significantly close to threshold. The energy dependence can be explained by the strong final state interaction. The large $\eta{}^3$He scattering length, assuming a negative value for its real part as indicated by a calculation using an optical potential, suggests the possibility of an $\eta{}^3$He quasibound state [9]. This conclusion is however challenged by recent calculations of the $\eta{}^3$He scattering length [16], using

multiple scattering theory, the validity of Eq. (11) being also questioned.

The $pd \rightarrow {}^3\mathrm{He}\,\eta$ reaction near threshold is well suited to produce η mesons. With a 7 mm thick LD_2 target, the optimum energy region for high intensity and low background is $\Delta T_p \sim 1-2$ MeV. The η yield in that case is $10^{-8}\,\eta$ per incident proton, so that $10^4\,\eta$/s could be produced with the maximum beam intensity of 10^{12} p/s which can be obtained at the Saturne II synchrotron. For a thicker target the beam energy has to be increased to compensate for the larger energy loss. For a 70 mm target, for example, the optimal energy would be $\Delta T_p = 4$ MeV. The increase in background in the larger region of phase space is roughly compensated by the smaller contamination by beam interactions in the target windows. A rate of $10^5\,\eta$/s would be obtained, with no substantial change in background level.

The Saturne tagged η facility allows the study of rare decay modes of the η meson with a sensitivity several orders of magnitude higher than achieved previously. So far the branching ratios for $\eta \rightarrow \mu^+\mu^-$ [13] and $\eta \rightarrow \gamma\gamma$ [17] have been measured. In these measurements the capabilities of the η facility have not been fully exploited yet, due to rate limitations in the detection systems for the η decay products.

ACKNOWLEDGMENTS

The authors have profited from many discussions with C. Wilkin. The Saturne staff is gratefully acknowledged for the high quality beam. We thank J. P. Robert, J. LeMeur, and B. Gonel for the technical support received during the experiment. For this research W.B., A.P., and W.W.J. in part, were supported by the U.S. National Science Foundation and R.A. and W.T.H.v.O by the North Atlantic Treaty Organization.

[1] J. Berger *et al.*, Phys. Rev. Lett. **61**, 919 (1988); F. Plouin *et al.*, in *Production and Decay of Light Mesons*, edited by P. Fleury (World Scientific, Singapore, 1988), p. 114.
[2] J.M. Laget and J.F. Lecolley, Phys. Rev. Lett. **61**, 2069 (1988).
[3] J.F. Germond and C. Wilkin, J. Phys. G **15**, 437 (1989).
[4] B. Mayer *et al.*, in *Intersections between Particle and Nuclear Physics*, Tucson 1991, edited by W.T.H. van Oers, AIP Conf. Proc. No. 243 (AIP, New York, 1991), p. 462; M. Garçon *et al.*, in *Proceedings of the 7th Lake Louise Winter Institute*, edited by B.A. Campbell *et al.* (World Scientific, Singapore, 1992), p. 337.
[5] H. Quéchon, Thèse de Doctorat de l'Université d'Orsay, 1980.
[6] A. Moalem, F. Meot, G. Leleux, J.P. Penicaud, A. Tkatchenko, and P. Birien, Nucl. Instrum. Methods A **289**, 168 (1990); Saturne User's Handbook: ''Manuel des Utilisateurs,'' 1991 (unpublished).
[7] R. Kessler, Ph.D. thesis, UCLA 1992.
[8] M.A. Pickar *et al.*, Phys. Rev. C **46**, 397 (1992); A. Boudard *et al.*, Nouv. Saturne **17**, 67 (1993).
[9] C. Wilkin, Phys. Rev. C **47**, R938 (1993).
[10] A. Moalem, E. Gedalin, L. Radolskaja, and Z. Shorer, Nucl. Phys. **A589**, 649 (1995).
[11] M. Goldberger and K.M. Watson, *Collision Theory* (Wiley, New York, 1964).
[12] G. Fäldt and C. Wilkin, Nucl. Phys. **A587**, 769 (1995).
[13] R. Abegg *et al.*, Phys. Rev. D **50**, 92 (1994).
[14] C. Wilkin, in *Production and Decay of Light Mesons*, edited by P. Fleury (World Scientific, Singapore, 1988), p. 187.
[15] The authors are grateful to C. Wilkin for raising this point.
[16] S. Wycech, A.M. Green, and J.A. Niskanen, Phys. Rev. C **52**, 544 (1995).
[17] R. Abegg *et al.*, Phys. Rev. D **53**, 11 (1996).